Protein corona formation on epigallocatechin gallate-Au nanoparticles suppressed tumor accumulation

Wakayama, Chihiro ; Inubushi, Sachiko ; Kunihisa, Tomonari ; Mizumoto, Sachiko ; Baba, Motoi ; Tanino, Hirokazu ; Cho, Ik Sung ; Ooya, Tooru

(Citation)
JCIS Open,9:100074

(Issue Date)
2023-04

(Resource Type)
journal article

(Version)
Version of Record

JCIS Open 9 (2023) 100074

Contents lists available at ScienceDirect

JCIS Open

journal homepage: www.journals.elsevier.com/jcis-open

Protein corona formation on epigallocatechin gallate-Au nanoparticles suppressed tumor accumulation

Chihiro Wakayama [a], Sachiko Inubushi [b], Tomonari Kunihisa [b], Sachiko Mizumoto [b], Motoi Baba [b], Hirokazu Tanino [c], Ik Sung Cho [d], Tooru Ooya [a,e,*]

[a] Graduate School of Engineering, Department of Chemical Science and Engineering, Kobe University, 1-1 Rokkodai-cho, Nada-ku, Kobe, 657 8501, Japan
[b] Division of Breast and Endocrine Surgery, Graduate School of Medicine, Kobe University, 7-5-1 Kusunoki-cho, Chuo-ku, Kobe, 650-0017, Japan
[c] Division of Breast Surgery, Department of Surgery, Wakayama Medical University, 811-1 Kimiidera, Wakayama-shi, 641-8509, Japan
[d] Department of Bioengineering, University of Illinois at Chicago, 1200 W Harrison St, Chicago, IL, 60607, USA
[e] Center for Advanced Medical Engineering Research & Development (CAMED), Kobe University, 1-5-1 Minatojima-minamimachi, Chuoku, Kobe, 657-0047, Japan

ARTICLE INFO

Handling Editor: Prof Qiang He

Keywords:
Epigallocatechin-3-gallate
Gold nanoparticles
Sodium alginate
Cellular uptake
Intravenous injection
Biodistribution

ABSTRACT

Metal nanoparticles (NPs), such as gold NPs (AuNPs), are particularly sensitive to X-rays, and thus specific accumulation of AuNPs in a tumor would allow radiotherapy with low energy X-rays and reduced side effects. AuNPs can be generated using $HAuCl_4$ and the natural polyphenol epigallocatechin-3-gallate (EGCG) in the presence of citrate. Here, we generated EGCG-AuNPs in the presence of several additives and examined the accumulation of these NPs in mouse tumors following intravenous administration. EGCG-AuNPs 15 nm in diameter in the presence of sodium alginate accumulated more in tumors compared to 40-nm-diameter EGCG-AuNPs. Furthermore, the results of *in vitro* cellular uptake and serum protein absorption studies suggest that adsorption of 15–16 kDa serum proteins to EGCG-AuNPs suppresses accumulation in tumors. Thus, tendency to adsorb specific proteins on EGCG-AuNPs surface should be tailored for enhancing their accumulation in tumors.

1. Introduction

Nanomaterials are of significant interest in cancer therapy because of their unique property of accumulating in cancer cells, resulting from the enhanced permeability and retention (EPR) effect [1]. Also, nanomaterials have a high surface-to-volume ratio and thus can be modified with various ligands to exhibit active targeting, high solubility, and/or high stability [1]. Metal nanoparticles (NPs) such as silver and gold NPs (AuNPs) are particularly sensitive to X-rays, and thus specific accumulation of metal NPs in a tumor allows radiotherapy with low energy X-rays and reduced side effects [2,3]. Colloidal or clustered particles of AuNPs with diameters of a few to several hundred nanometers are of interest because of four unique properties [2]. The first is their good biocompatibility and low toxicity [4]. The second is the ease of controlling their size and shape: by using different reducing or stabilizing agents, the particle size can be controlled between several nanometers to 200 nm, and shapes such as nanospheres, nanorods, nano-stars, and nano-cubes can be generated [2,4]. The third is the ease and versatility of surface modifications. Gold surfaces can be modified with thiol and amino groups, allowing the ready modification of AuNPs with proteins, peptides, DNA, chemical/biological polymers, and a variety of other molecules [2,5,6]. Surface modifications are critical for biocompatibility and stability under biological conditions and can provide NPs that actively target tumors, so this property is vital for the medical use of nanomaterials. The fourth is their optoelectronic properties, useful for surface plasmon resonance (SPR) and high X-ray and near-infrared (NIR) absorption. In SPR, illumination at resonant wavelengths delocalizes conduction band electrons on the AuNP surface, which undergo collective oscillation. The light is then absorbed/scattered by the AuNPs, inducing a wide variety of optical phenomena [7].

There are several methods for preparing AuNPs, of which the citrate reduction method is classified as a green nanoscience method [8]. This very simple method does not use organic solvents or generate undesirable side products [8]. Sodium citrate acts as a reducing and stabilizing agent and generates AuNPs 5–40 nm in diameter [9]. Au(III) is reduced to Au(I) in two steps, then Au(I) forms a multimolecular complex with

* Corresponding author. Graduate School of Engineering, Department of Chemical Science and Engineering, Kobe University, 1-1 Rokkodai-cho, Nada-ku, Kobe, 657 8501, Japan.
E-mail address: ooya@tiger.kobe-u.ac.jp (T. Ooya).

https://doi.org/10.1016/j.jciso.2023.100074
Received 22 August 2022; Received in revised form 25 December 2022; Accepted 1 January 2023

dicarboxyacetone molecules present in the solution. This is followed by the generation of Au (0) [10], which functions as seeds for $AuCl_4^-$ absorption and subsequent growth of the AuNPs [11].

Similarly, polyphenol can be used as a reducing and stabilizing agent. Sanna et al. reported using the natural polyphenols epigallocatechin-3-gallate (EGCG), resveratrol (RSV) and fisetin (FS) to prepare AuNPs, and characterized the properties of polyphenol-coated AuNPs [12]. For example, EGCG-AuNPs prepared by using EGCG as a reducing and stabilizing agent have multiple potential uses for cancer treatment [13–18]. Sanna et al. reported that EGCG-AuNPs induced a dose-dependent reduction of SH-SY5Y-CFP-DEVD-YFP cell viability, similar to that of free EGCG, and showed the utility of EGCG-AuNPs as a cancer treatment drug [12]. Chavva et al. recently reported that EGCG-AuNPs were taken up much more readily by cancer cells compared to normal cells, and that EGCG-AuNPs actively target the 67LR receptor [16]. Similarly, citrate-AuNPs act as radiosensitizers and improve the efficacy of radiotherapy in tumor-bearing mice [19]. We previously reported the relationship between EGCG-AuNP size and cellular uptake, and revealed that the appropriate particle size for cellular uptake depended on the cell type. EGCG-AuNPs about 40 nm in diameter showed the best uptake by MDA-MB-231 cells and the uptake was mediated by the 67LR receptor [14]. Research to date indicates that EGCG-AuNPs likely exhibit active targeting, anti-tumor, and radiosensitizer characteristics, and function as combination therapy agents. However, there are few reports of *in vivo* experiments using EGCG-AuNPs. Shukla et al. reported that about 72% of EGCG-^{198}AuNPs were retained in tumors 24 h after intratumoral administration to tumor-bearing mice [20]. Hsieh et al. revealed that EGCG–AuNPs inhibited tumor cell growth by cell apoptosis after oral, intraperitoneal or intratumoral injection [17]. AuNPs 10, 50, 100, and 250 nm in diameter were prepared by citrate reduction of $HAuCl_4$ and most tended to accumulate in the liver, spleen and blood at 24 h after intravenous injection into rats [21]. Sonavane et al. similarly found that AuNPs regardless of size suspended in a solution of sodium alginate were mostly found in the liver [22]. However, to our knowledge, there are no reports regarding the biodistribution and tumor accumulation of EGCG-AuNPs administered via intravenous injection.

In this study, EGCG-AuNPs of two different sizes (15- and 40-nm) were prepared and their biodistribution and tumor accumulation following intravenous injection in mice were evaluated. The size-dependence of AuNP accumulation was tested by preparing 15-nm and 40-nm citrate-EGCG-AuNPs (Ci-EGCG-$AuNP_{15}$ or Ci-EGCG-$AuNP_{40}$) by changing the ratio of citrate and EGCG. Ci-EGCG-$AuNP_{15}$ and Ci-EGCG-$AuNP_{40}$ were characterized by transmission electron microscope (TEM) observation, dynamic light scattering (DLS) measurements and quantification of the amount of EGCG. Sodium alginate and dextran were investigated as additives to improve the stability of the Ci-EGCG-AuNPs under physiological conditions. The stabilization, cellular uptake and tumor accumulation of Ci-EGCG-$AuNPs_{15/40}$ in 10 wt% dextran solution and 0.1 wt% sodium alginate solution were compared. It is known that dextran has been used as a plasma expander at 6–10 wt % [23] and as a stabilizing agent of metal nanoparticles [24]. In addition, sodium alginate (0.5 wt%) has been also used as a suspending agent for intravenous injection to mice [22]. We found that Ci-EGCG-$AuNP_{15}$ dispersed in sodium alginate solution showed better accumulation in tumors. However, the accumulation was not significant level due to serum protein corona formation. We suggest here that, in order to success intravenous injection of Ci-EGCG-AuNPs, the protein corona formation must be prevented.

2. Materials and methods

2.1. Materials

Hydrogen tetrachloroaurate (III) tetrahydrate ($HAuCl_4{\cdot}4H_2O$), potassium carbonate, gold standard solution (Au 1000), sodium alginate 300–400, ammonium peroxodisulfate (APS), 2-mercaptoethanol, *N,N,N′,N′*-tetramethylethylenediamine (TEMED), and a Silver Stain 2 kit were purchased from FJIFILM Wako Pure Chemical Corporation (Osaka, Japan). (−)-Epigallocatechin gallate and fetal bovine serum (FBS) were purchased from Sigma-Aldrich Co. LLC. (St. Louis, MO, USA). Dulbecco's Modified Eagle Medium (DMEM), Dulbecco's phosphate-buffered saline (DPBS), accutase, penicillin-streptomycin mixed solution (stabilized) and sodium dodecyl sulfate (SDS) were purchased from Nacalai Tesque, Inc. (Kyoto, Japan). Dextran 40 was purchased from Tokyo Chemical Industry Co. Inc. (Tokyo Japan). Unstained protein standards were purchased from Bio-Rad Laboratories, Inc. (Hercules CA, USA).

2.2. Measurements

A PPS-5510 organic synthesizer (Tokyo Rikakikai Co. Ltd., Tokyo, Japan) was used to prepare the AuNPs. A micro-ultracentrifuge (CS 150GXII, Eppendorf Himac Technologies Co., Ltd., Hitachinaka, Japan) was used to separate and purify the AuNPs. UV–vis absorption spectra were obtained using a V-730 UV–visible/NIR spectrophotometer (JASCO Corporation, Tokyo, Japan). Zetasizer Nano from Malvern Panalytical Ltd. (Worcestershire, UK) was used for DLS measurements, and Malvern Zetasizer software was used for data analysis. A high performance liquid chromatography (HPLC) system comprising a GILSON 119UV/VIS detector, GILSON 231XL autosampler, GILSON 805 manometric module, GILSON 811c dynamic mixer and a GILSON DILTOR401 injector (Gilson, WI, USA). The column was a COSMOSIL 5C18-MS-II (Φ4.6 nm × 150 mm) (Nacalai Tesque, Inc., Kyoto, Japan) and the data were analyzed using Unipoint Version 3.3 (Gilson, WI, USA). A Hitachi H-7650 (120 kV) (Hitachi High-Tech Corporation, Tokyo, Japan) was used for TEM observation. Gold was analyzed using inductively coupled plasma atomic emission spectroscopy (ICP-AES) (SPS3100, (Hitachi High-Tech Co., Tokyo, Japan). A hot dry bath (HDB-2N, ASONE Corporation, Osaka, Japan) was used for dissolving organs. A PowerPac universal power supply (Bio-Rad Laboratories, Inc., CA, USA) was used for SDS-PAGE.

2.3. Preparation and characterization of Ci-EGCG-AuNPs

A mixture of 4 mM $HAuCl_4$ (1 ml) and 8.4 ml of DI water, and a mixture of 1% $Na_3C_6H_5O_7$ (125 μl), 2.5% EGCG (154, or 462 μl), 25 mM K_2CO_3 (125 μl) and DI water were separately warmed to 60 °C and then mixed while stirring. After the mixture turned red, the mixture was heated to 95 °C under stirring and then cooled on ice. The particles were washed twice and re-dispersed using DI water. The concentration of gold was determined using ICP-AES.

2.4. Quantification of EGCG loading in the Ci-EGCG-AuNPs

The concentration of gold in the Ci-EGCG-AuNPs was measured by ICP-AES (wavelength: 242.795 nm) and the amount of EGCG was determined by HPLC. Elution was carried out using aqueous phosphoric acid (20 mmol, pH 2.5) and methanol (80:20 v/v) as the mobile phase at a flow rate of 1.0 ml/min. The UV detection wavelength was 254 nm. A calibration curve was constructed using a series of EGCG solutions (10, 20, 50, 80, 100, 200, 300, 400 μg/ml). The supernatant of the preparation mixture after centrifugation was separated by HPLC, and the EGCG content in the supernatant was calculated from the calibration curve. The EGCG content of the Ci-EGCG-AuNPs was calculated using the following equation:

$$\omega_{EGCG} = \frac{\Delta m_{EGCG}}{m_{Au}}$$

where ω_{EGCG} is the EGCG content (mg EGCG/mg AuNPs), Δm_{EGCG} is the EGCG content on the Au surface ($m_{total\ EGCG\ feed\ consumption}$ (mg) − $m_{EGCG\ in\ supernatent}$(mg)), and m_{Au} is the amount of gold in the EGCG-AuNPs.

2.5. Characterization of the Ci-EGCG-AuNPs

Nanoparticle size was characterized by DLS. All measurements were obtained in triplicate in DI water at 25 °C with an angle of detection of 173°. Images were recorded digitally with Zetasizer software. UV–vis absorption spectra of 0.05 mg/ml samples dispersed in DI water were measured between 350 and 700 nm. The morphology of EGCG-AuNPs$_{15/40}$ was characterized by TEM observation by dropping the samples (Au concentration 0.25 mg/ml in DI water) on thick carbon film-coated TEM grids (Cu, 200 mesh) and drying in a vacuum drier overnight.

2.6. Stability tests

The Ci-EGCG-AuNPs$_{15/40}$ were adjusted to a concentration of 0.05 mg (Au)/ml with DPBS, 10 wt% dextran-DPBS, FBS-DPBS, 10 wt% dextran-FBS-DPBS or 2 wt% sodium alginate-FBS-DPBS (the ratio of FBS:DPBS was 1:1 for all conditions). Then, the solutions were heated at 60, 70 or 80 °C for 6 h and the UV–vis spectra were acquired before and after heating.

2.7. In vivo tests using tumor-bearing mice

This study was approved and carried out by the Oriental Bio Service Animal Experimentation Regulations. Six-week-old female BALBc nu/nu mice were obtained from Oriental Bio Service Inc. (Kobe, Japan). MDA-MB-231 cells (5×10^6 cells/mouse) were injected subcutaneously to establish tumor-bearing mice. Small pieces of harvested subcutaneous tumor were then transplanted into the mammary gland of the nude mice. The tumors were allowed to grow to about 1 cm in diameter. Ci-EGCG-AuNPs$_{15/40}$ were dispersed in 0.1 wt% sodium alginate-DPBS (Au concentration: 5 mg/ml) or 10 wt% dextran-DPBS (Au concentration: 5 mg/ml) and administrated by intravenous injection (100 μl). The mice were sacrificed 60 min after injection and tumor left and right, blood, lung, liver, spleen, kidney, heart and tail were collected. The amount of accumulated Au in each organ was measured by dissolving the organ in 1 ml of aqua regia and each sample was diluted with DI water to 5 ml. The gold content in these samples was analyzed by ICP-AES.

2.8. Cellular uptake of Ci-EGCG-AuNP$_{15}$

MDA-MB-231 cells were seeded in 6-well plates at a density of 2×10^5 cells per well (2 ml RPMI 1640 for each well). After 24 h incubation, the medium was replaced by a mixture of RPMI 1640 (1.9 ml) and Ci-EGCG-AuNP$_{15}$ (final gold concentration was 0.75 μg/ml, NPs were dispersed in 100 ml of 10 wt% dextran-DPBS, 5 wt% dextran-DPBS, 0.1 wt% sodium alginate-DPBS, or DPBS). The cells were treated for 6 h or 24 h, rinsed twice with warm DPBS, harvested using accutase and counted. Aqua regia (1 ml) was then added to the cells and the solution was heated at 80 °C for 3 h. The samples were further diluted with DI water to a total volume of 5 ml and the total gold content was analyzed by ICP-AES.

2.9. Protein absorption on Ci-EGCG-AuNP$_{15}$

Ci-EGCG-AuNP$_{15}$ was incubated in 50% FBS-Tris-HCl, 70% FBS-Tris-HCl, 50% FBS-Tris-HCl-10 wt% dextran, 70% FBS-Tris-HCl-10 wt% dextran, 50% FBS-Tris-HCl-0.1 wt% sodium alginate, or 70% FBS-Tris-HCl-0.1 wt% sodium alginate (Au concentration: 75 μg/ml, Tris-HCl contained 0.15 M NaCl and 1 mM EDTA) for 1 h and centrifuged for 20 min (22,000 rpm, 20,454×*g*). The obtained NPs were washed with 10 mM Tri-HCl (pH 7.5) and 0.15 M NaCl. Bound proteins were removed from the NPs by mixing with 1% mercaptoethanol-SDS-loading buffer, then separating the buffer and NPs by centrifugation. Finally, the solutions containing bound proteins were analyzed by SDS-PAGE (15% gel), then the gels were stained using a silver stain 2 kit (Wako) by following the manufacturer's instructions.

3. Results and discussion

Small NPs were prepared using EGCG and sodium citrate as reducing and stabilizing agents. Varying the initial amount of EGCG provided two types of Ci-EGCG-AuNPs. Each sample was wine-red to blue-red in color (Fig. 1), typical of Au colloids, and the NPs were characterized by DLS, HPLC, and ICP-AES.

no. 2 (see: Table 1).

The Z-average diameter increased in proportion to the feed amount of EGCG (Table 1), indicating that the balance between a weak reducing agent and a strong reducing agent affects particles size. Because EGCG is unstable and easily oxidizes under high pH conditions, EGCG is a weak reducing agent compared to sodium citrate. HPLC measurements showed that the EGCG concentration in the preparation mixture supernatants after centrifugation decreased compared to the initial EGCG concentration, indicating that EGCG acted as a reducing agent and was absorbed on the surface of the AuNPs. The EGCG content of the AuNPs was calculated (Table 1). Both samples contained over 0.81 mg/mg EGCG, indicating that the AuNPs were saturated with loaded EGCG. The particle size was affected by the balance of the stronger reducing agent (citrate) and weaker reducing agent (EGCG), with a tendency to bigger particles when the ratio of the weaker reducing agent was higher.

To investigate the effect of particle size on accumulation in tumors, AuNPs prepared using conditions no. 1 and no. 2 were studied further and named Ci-EGCG-AuNPs$_{15/40}$. The morphology of Ci-EGCG-AuNPs$_{15/40}$ was further investigated by TEM observation and by UV–vis. TEM images (Fig. 2(a and b)) showed that both Ci-EGCG-AuNP$_{15}$ and Ci-EGCG-AuNP$_{40}$ were spherical, with an average diameter of 5.6 nm and 7.6 nm, respectively, and were smaller than the Z-average diameter. Since the Z-average size is calculated using Cumulants analysis, which assumes a single particle size, most particles are actually smaller than the Z-average size. Also, aggregation can result in bigger Z-average diameters. The UV–vis spectra of Ci-EGCG-AuNPs$_{15/40}$ are shown in Fig. 2(c). Unique Au absorbance bands were observed by SPR, and the red shift of the maximum absorption wavelength corresponded with the increasing size of the AuNPs.

NPs easily aggregate in, for example, the presence of salts, extreme pH and at high temperature. Dextran 40 and sodium alginate were thus used

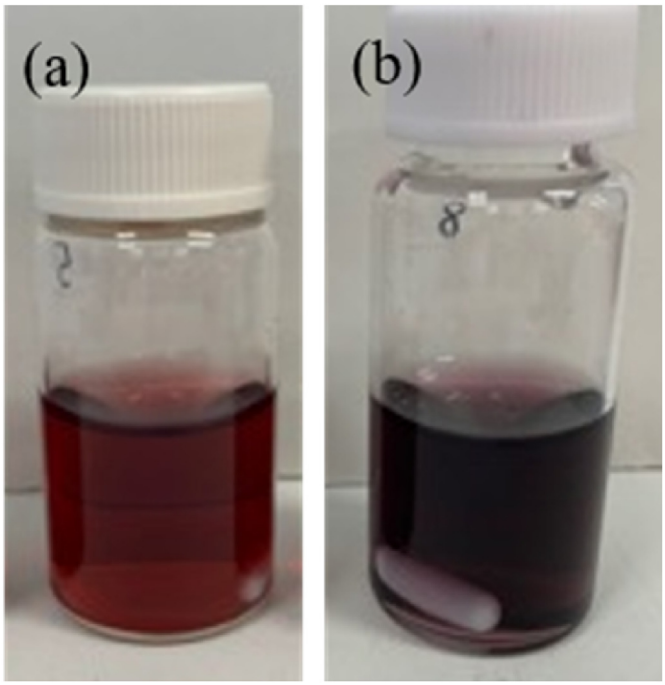

Fig. 1. Photograph of Ci-EGCG-AuNP dispersions prepared using different amounts of EGCG. Condition (a) no. 1, (b).

Table 1
Z-average diameter, Zeta potential, PdI and EGCG content of each condition.

Condition no. (Citrate/EGCG)	Z-average diameter [nm]	Zeta potential [mv]	PdI[a)]	EGCG content[b)] (mg EGCG/mg AuNPs)
1 (1:2)	14.9	−7.22	0.619	0.848 ± 0.005
2 (1:6)	42.4	−24.4	0.597	0.853 ± 0.007

[a)] PdI: Polydispersity Index.
[b)] Determined by HPLC (mean ± SEM, n = 3).

as additives in the dispersion solutions to investigate the excluded volume effect [25]. Both compounds are biocompatible materials and so should not cause adverse effects when used *in vitro* and *in vivo*. The dispersion solutions were heated to promote the aggregation of AuNPs and to compare the stability of the NPs under each condition.

When Ci-EGCG-AuNP$_{15}$ was dispersed in DPBS, the absorption peaks became smaller and disappeared, depending on the temperature, due to aggregation of the NPs (Fig. 3(a)), as observed in the photos. Before heating, Ci-EGCG-AuNP$_{15}$ was uniformly dispersed in DPBS and gave a red color, but when the NPs aggregated and precipitated, the color was blue-black. In contrast, when Ci-EGCG-AuNP$_{15}$ was dispersed in 10 wt% dextran-DPBS solution, some NP aggregation was observed after heating at 80 °C but the maximum absorption wavelength and red color were maintained (Fig. 3(b)). These results indicate that the stability of the NPs was improved by adding dextran 40 to the dispersion solution. A similar tendency was observed when Ci-EGCG-AuNP$_{40}$ were used (data not shown).

To investigate the stability of Ci-EGCG-AuNPs$_{15/40}$ in a more biomimetic environment, the NPs were dispersed in FBS-DPBS (1:1) solution and the stability upon heating was measured by UV–vis. All NPs in FBS-DPBS showed higher stability compared to in DPBS, indicating that protein absorption to NPs improves the stability of NPs. Fig. 4(a) shows that the maximum absorption wavelength of Ci-EGCG-AuNP$_{15}$ in FBS-DPBS was red-shifted by heating, whereas the maximum absorption wavelength of NPs dispersed in a solution containing dextran 40 and sodium alginate remained unchanged after heating (Fig. 4(b and c)), indicating that Ci-EGCG-AuNP$_{15}$ was stabilized by the addition of dextran or sodium alginate in this biomimetic environment. The photos in Fig. 4(b and c) show that the NPs in the presence of polysaccharides, especially sodium alginate, tended to promote protein denaturation, making it impossible to measure the UV–vis spectra. Zhao et al. reported that heat-denatured albumin and alginate forms aggregates, the main driving force of which is the electrostatic interactions between the oppositely charged amino acids and the anionic polysaccharide, keeping its secondary structure [26]. Based on this report, the heat-induced aggregation as seen in Fig. 4(b and c) is considered to be the same reason. The stabilization effect of dextran and sodium alginate must therefore be studied *in vivo*. Similar observations were obtained using Ci-EGCG-AuNP$_{40}$ (data not shown), showing that both dextran and sodium alginate stabilized Ci-EGCG-AuNPs$_{15/40}$ in the biomimetic environment.

The effect of NP size and additives on *in vivo* accumulation in tumors was evaluated by animal experiments. The accumulation of Ci-EGCG-AuNPs$_{15/40}$ in each organ and tumor is shown in Fig. 5. Although the obtained each organ's data was just twice average, we tried to discuss the tendency of accumulation of Ci-EGCG-AuNPs$_{15/40}$. There was high accumulation in lung, liver, and spleen, and little accumulation in tumors. Comparison of the amount of Au accumulated in the tumors showed that more Ci-EGCG-AuNP$_{15}$ accumulated than Ci-EGCG-AuNP$_{40}$, and that Ci-EGCG-AuNP$_{15}$ dispersed in 0.1 wt% sodium alginate-DPBS

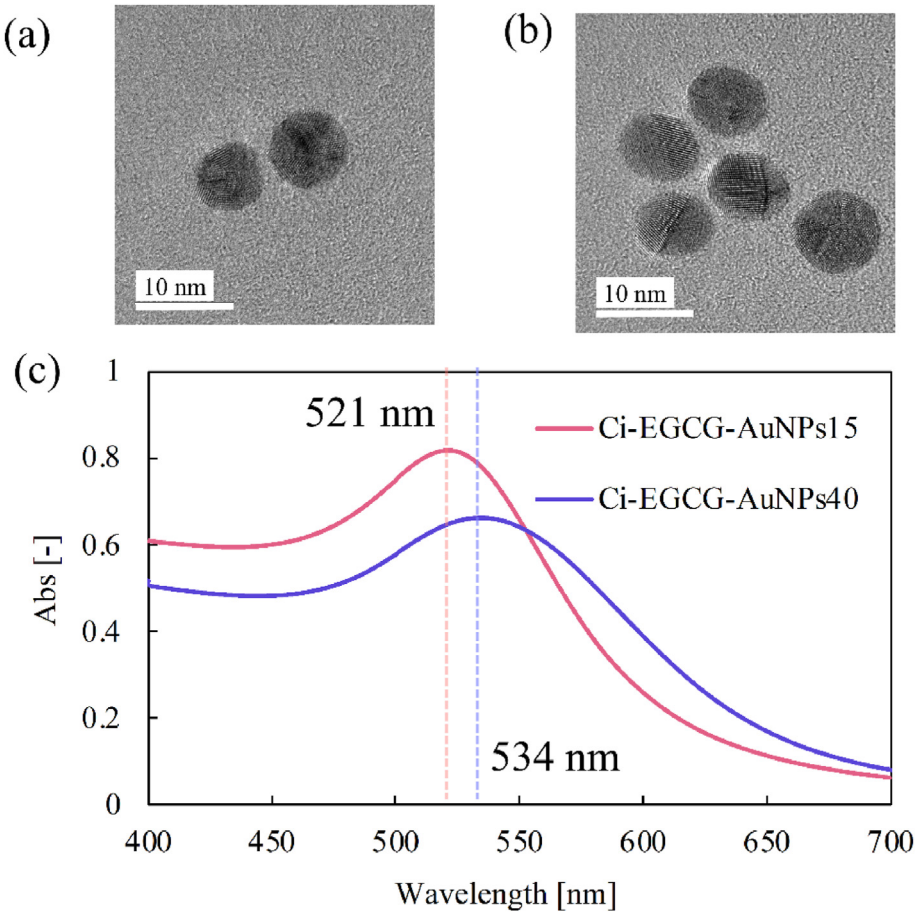

Fig. 2. TEM image of (a) Ci-EGCG-AuNPs$_{15}$ and (b) Ci-EGCG-AuNPs$_{40}$, and (c) UV–vis spectra of Ci-EGCG-AuNPs$_{15/40}$ in water (Au concentration: 0.05 mg/ml).

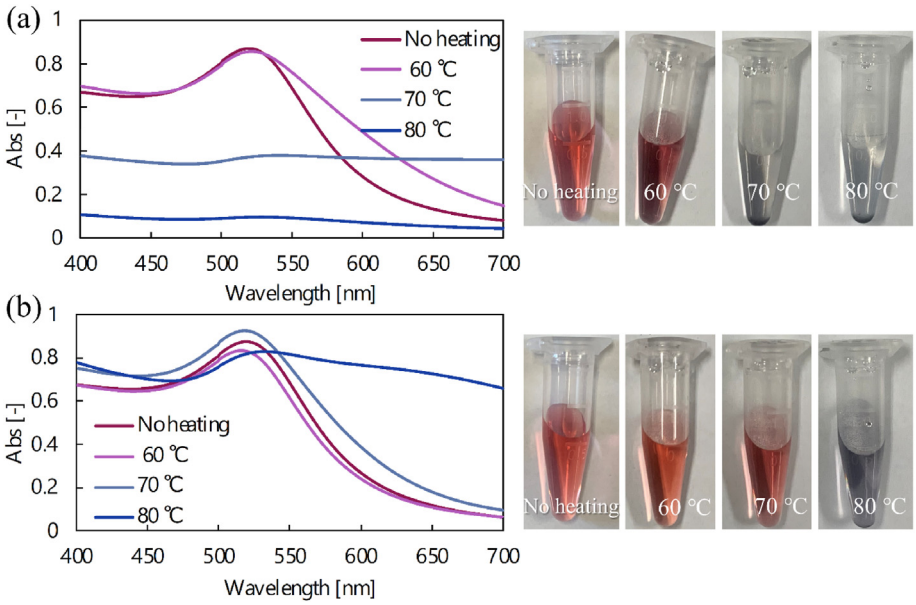

Fig. 3. UV–vis spectra and photos of Ci-EGCG-AuNPs$_{15}$ in (a) DPBS, (b) 10 wt% dextran-DPBS (Au concentration: 0.05 mg/ml).

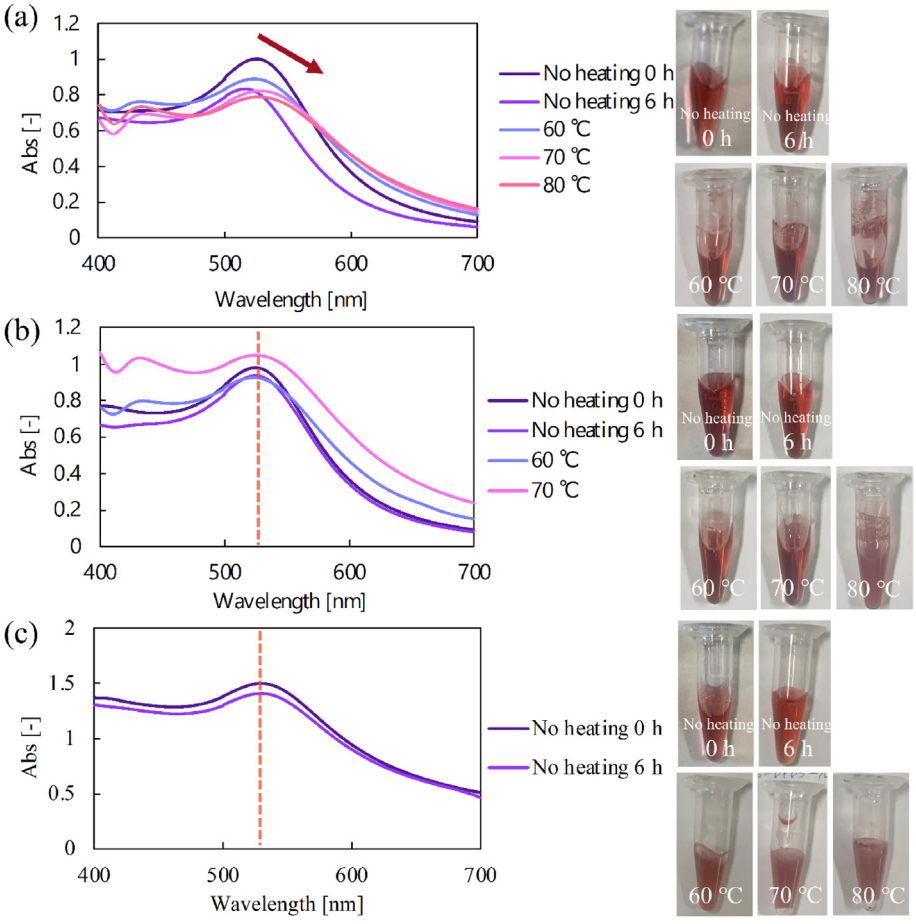

Fig. 4. UV–vis spectra and photos of Ci-EGCG-AuNP$_{15}$ in (a) FBS-DPBS, (b) 10 wt% dextran-FBS-DPBS, (c) 2 wt% sodium alginate-FBS-DPBS (Au concentration: 0.05 mg/ml).

showed the highest accumulation (Fig. 6). Thus, Ci-EGCG-AuNP$_{15}$ is more likely to accumulate in tumors, and a dispersion solution containing sodium alginate likely promotes the accumulation of Ci-EGCG-AuNP$_{15}$. This accumulation behavior *in vivo* is in conflict with our previous report, which showed that EGCG-AuNPs were taken up by MDA-MB-231 cells [14], indicating the importance of environmental differences between *in vitro* and *in vivo* conditions. Many types of biological molecules such as proteins are one big difference between *in vitro* and *in vivo* conditions,

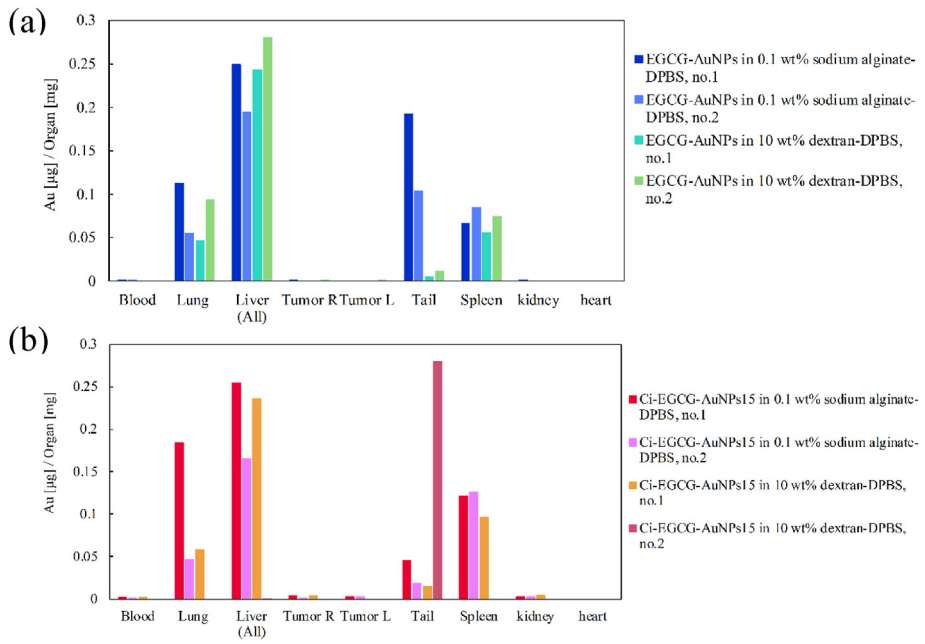

Fig. 5. Accumulated amount of Au in organs and tumors using (a) Ci-EGCG-AuNP$_{40}$, (b) Ci-EGCG-AuNP$_{15}$. MDA-MB-231 cells (5×10^6 cells/mouse) were injected subcutaneously to establish tumor-bearing mice (n = 2, Mean).

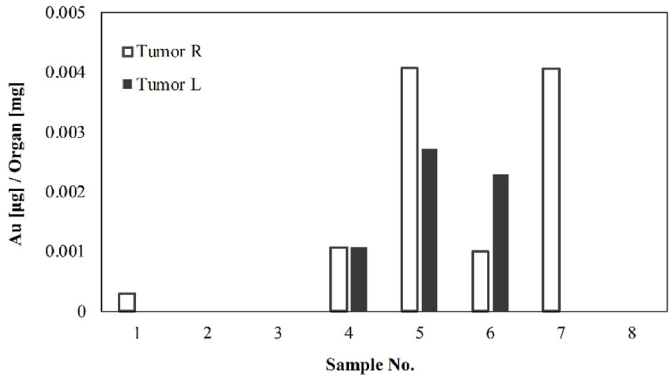

Fig. 6. Accumulated amount of Au in tumors (Sample no. 1–2: Ci-EGCG-AuNP$_{40}$ in 0.1 wt% sodium alginate-DPBS, no. 3–4: Ci-EGCG-AuNP$_{40}$ in 10 wt% dextran-DPBS, no. 5–6: Ci-EGCG-AuNP$_{15}$ in 0.1 wt% sodium alginate-DPBS, no. 7–8: Ci-EGCG-AuNP$_{15}$ in 10 wt% dextran-DPBS) (n = 2, Mean).

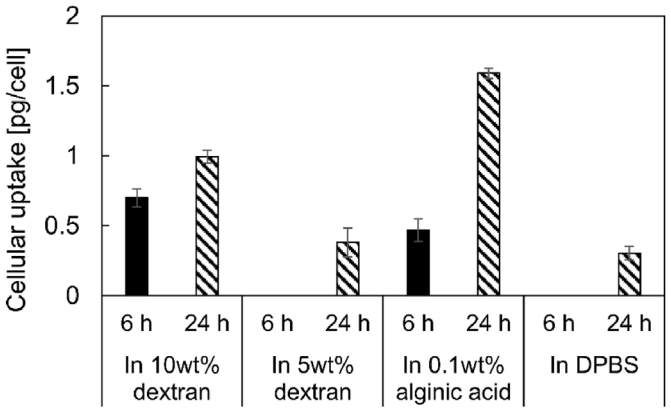

Fig. 7. Cellular uptake of Ci-EGCG-AuNPs$_{15}$ toward MDA-MB-231 cells in RPMI1640 containing 10% FBS at 37 °C for 6 h (closed bar) and 24 h (stripped bar): final gold concentration was all 75 μg/ml, Ci-EGCG-AuNP15 was dispersed in 10 wt% dextran-DPBS, 5 wt% dextran-DPBS, 0.1 wt% sodium alginate-DPBS, or DPBS) (n = 3, Mean ± S.E.M.).

because protein absorption to NPs changes the size and surface conditions of the particles. We thus selected only Ci-EGCG-AuNP$_{15}$ to further analyze the relationship between cellular uptake and serum protein absorption using MDA-MB-231 cells.

The cellular uptake of Ci-EGCG-AuNP$_{15}$ was investigated using ICP-AES, and the condition of the cells after uptake was observed. Quantified Au amounts of all the samples were below 1.7 pg/cell, which was calculated below 0.2% of cellular uptake rate (Fig. 7). This result suggests that cellular uptake was reduced in the FBS-containing medium. Lin et al. reported that FBS-coated AuNPs form protein corona, which reduces aggregation of AuNPs and decreases cellular uptake amount [27]. Considering this report, the obtained results (Fig. 7) are likely to be correlated with protein corona formation in RPMI1640 containing 10% FBS. Although the cellular uptake amount was low, Ci-EGCG-AuNP$_{15}$ dispersed in sodium alginate-DPBS were taken up a little bit better than Ci-EGCG-AuNP$_{15}$ dispersed in dextran-DPBS or DPBS (Fig. 7), showing that 10 wt% dextran and sodium alginate likely facilitates cellular uptake, which is also should be considered with protein corona formation.

SDS-PAGE analysis (15% gel) was used clarify serum protein absorption to Ci-EGCG-AuNP$_{15}$ using 50 or 70% FBS-Tris buffer to simulate the blood environment. Protein absorption to Ci-EGCG-AuNPs$_{15}$ depended on the FBS concentration and the additives present. Fig. 8 shows that many different molecular weight proteins were absorbed to the Ci-EGCG-AuNP$_{15}$ samples and the absorption behavior was not related to the FBS concentration: Middle-molecular-weight proteins (100-35 kDa) in FBS including BSA and fibrinogen, the most represented proteins in FBS, were strongly adsorbed after 1 h incubation. This phenomenon was not consistent with previous report: BSA and fibrinogen was partially interacted with NP surface, and highly affine proteins competitively adsorbed on the surface [28]. This result suggests that EGCG-modification of AuNP surface enhanced adsorption of middle-molecular-weight proteins, and those protein coronas decreased cellular uptake amount. It is noted that approximately 20–25 kDa bands were reduced in the presence of dextran and sodium alginate (Fig. 8). These results suggest that these polysaccharide additives are worthful for preventing some proteins around 20–25 kDa corona formation. Furthermore, a strong approximately 15–16 kDa band appeared only

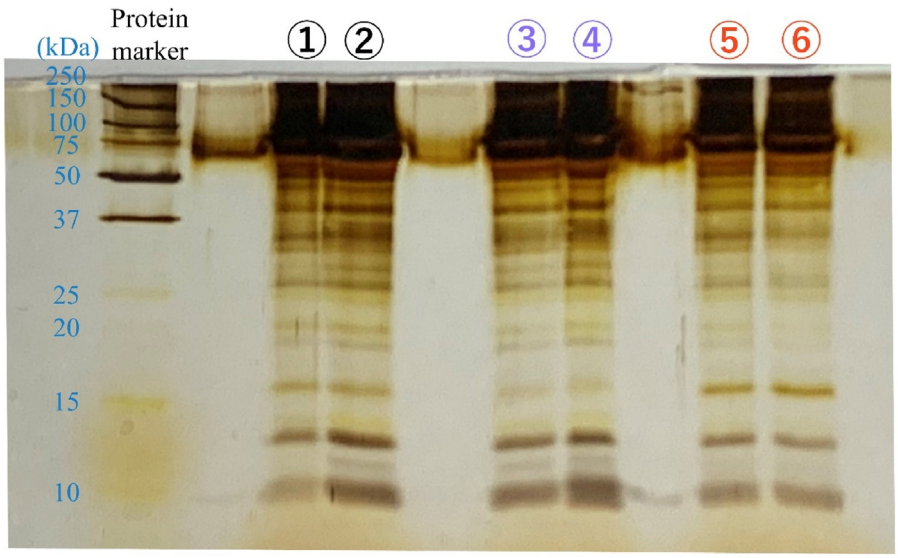

Fig. 8. SDS-PAGE (15% gel) of proteins absorbed to Ci-EGCG-AuNP$_{15}$ for 1 h incubation (incubated solution conditions: ① 50% FBS-Tris buffer, ② 70% FBS-Tris buffer, ③ 10 wt% dextran-50% FBS-Tris buffer, ④ 10 wt% dextran-70% FBS-Tris buffer, ⑤ 0.1 wt% sodium alginate-50% FBS-Tris buffer, ⑥ 0.1 wt% sodium alginate-70% FBS-Tris buffer).

when Ci-EGCG-AuNP$_{15}$ were incubated in a solution containing sodium alginate (Fig. 8). Given the observed accumulation behavior of Ci-EGCG-AuNP$_{15}$ in tumors (Fig. 6), sodium alginate might also promote the absorption of an approximately 15–16 kDa protein and this protein might affect NP accumulation in tumors. According to the proteomic information of fetal bovine serum (FBS) reported by Zheng et al. [29] and Sakulkhu et al. [30], predicted protein candidates of 15–16 kDa include hemoglobin subunit alpha (15.1 kDa), hemoglobin subunit beta (16.0 kDa), hemoglobin fetal subunit beta (15.9 kDa), and profilin-1 (15.0 kDa). If some of them are related to the enhanced cellular uptake in the presence of sodium alginate (Figs. 8), 15–16 kDa proteins might facilitate the uptake via sodium alginate-mediated protein adsorption. While sodium alginate can work as a biosorption agent, reductant, and stabilizer, sodium alginate was considered to stabilize Ci-EGCG-AuNP$_{15}$ by interacting with NPs as stabilizer [31]. Therefore, sodium alginate is considered to be located around the Ci-EGCG-AuNP$_{15}$ surface, presumably due to multivalent interaction between carboxy anions and Au atom. Of those candidates of 15–16 kDa proteins, hemoglobin subunit alpha (15.1 kDa), hemoglobin subunit beta (16.0 kDa), and hemoglobin fetal subunit beta (15.9 kDa) are considered the most likely, because hemoglobin and AuNPs are spontaneously interact with each other via hydrophobic interactions [32]. It is considered the hemoglobin subunits adsorbed EGCG-unmodified AuNP spaces bearing sodium alginate, and the resulted Ci-EGCG-AuNP$_{15}$ was likely to be taken up by endocytosis to tumor sites. It is known that tumor microenvironment exhibits acidic condition (pH 5.8–7.6) [33] and high ionic concentration [34], both of which tend to induce aggregation of nanoparticles [35]. Yan et al. reported that protein corona-coated AuNP with 20 nm diameter prevented an increase in aggregation and size in the tumor-mimicking microenvironment [36]. We consider that, in our case, the formed protein corona on Ci-EGCG-AuNP$_{15}$ is stable under tumor microenvironment.

4. Conclusion

EGCG-AuNP 15 nm in diameter in the presence of sodium alginate accumulated more in tumors after intravenous injection into mice compared to 40-nm-diameter EGCG-AuNP. The AuNP surface was modified with EGCG but no 67LR-mediated tumor accumulation was observed. The results of *in vitro* cellular uptake and serum protein absorption suggest that 15–16 kDa serum proteins including hemoglobin subunit alpha and beta facilitates NP accumulation in tumors in the presence of sodium alginate. The protein absorption to the particles should be carefully considered to enhance NP accumulation when the NPs are administered via intravenous injection into tumors.

Declaration of competing interest

The authors declare that they have no known competing financial interests or personal relationships that could have appeared to influence the work reported in this paper.

Data availability

Data will be made available on request.

Acknowledgements

We thank Miss Moemi Matsuda (Kobe University) to help cell culture studies. This study was financially supported by the Grant Program for the Creation of Local Universities and Regional Industries by the Cabinet Office, Government of Japan (Kobe vision for the healthcare of tomorrow), Hyogo Science and Technology Association, Japan (No. 2079), and the JSPS KAKENHI (Grant Nos. JP22H04545and 22K16462). This work was supported in part by "Advanced Research Infrastructure for Materials and Nanotechnology in Japan (ARIM)" of the Ministry of Education, Culture, Sports, Science and Technology (MEXT).

References

[1] S. Tran, P. DeGiovanni, B. Piel, P. Rai, Cancer nanomedicine: a review of recent success in drug delivery, Clin. Transl. Med. 6 (2017), https://doi.org/10.1186/s40169-017-0175-0.
[2] S. Her, D.A. Jaffray, C. Allen, Gold nanoparticles for applications in cancer radiotherapy: mechanisms and recent advancements, Adv. Drug Deliv. Rev. 109 (2017) 84–101, https://doi.org/10.1016/j.addr.2015.12.012.
[3] M.F. Attia, J. Wallyn, N. Anton, T.F. Vandamme, Inorganic nanoparticles for X-ray computed tomography imaging, Crit. Rev. Ther. Drug Carrier Syst. 35 (2018) 391–432, https://doi.org/10.1615/CritRevTherDrugCarrierSyst.2018020974.
[4] N. Elahi, M. Kamali, M.H. Baghersad, Recent biomedical applications of gold nanoparticles: a review, Talanta 184 (2018) 537–556, https://doi.org/10.1016/j.talanta.2018.02.088.
[5] D.L. Xia, Y.F. Wang, N. Bao, H. He, X. dong Li, Y.P. Chen, H.Y. Gu, Influence of reducing agents on biosafety and biocompatibility of gold nanoparticles, Appl.

Biochem. Biotechnol. 174 (2014) 2458–2470, https://doi.org/10.1007/s12010-014-1193-7.
[6] J. Woong Lee, S.-R. Choi, J. Hyuk Heo, Simultaneous stabilization and functionalization of gold nanoparticles via biomolecule conjugation: progress and perspectives, ACS Appl. Mater. Interfaces 13 (2021) 42311–42328, https://doi.org/10.1021/acsami.1c10436.
[7] N.S. Abadeer, C.J. Murphy, Recent progress in cancer thermal therapy using gold nanoparticles, J. Phys. Chem. C 120 (2016) 4691–4716, https://doi.org/10.1021/acs.jpcc.5b11232.
[8] J.A. Dahl, B.L.S. Maddux, J.E. Hutchison, Toward Greener Nanosynthesis, 2007, pp. 2228–2269, https://doi.org/10.1021/cr050943k.
[9] P. Slepička, N.S. Kasálková, J. Siegel, Z. Kolská, V. Švorčík, Methods of gold and silver nanoparticles preparation, Materials 13 (2020) 1, https://doi.org/10.3390/ma13010001.
[10] I. Ojea-Jiménez, F.M. Romero, N.G. Bastús, V. Puntes, Small gold nanoparticles synthesized with sodium citrate and heavy water: insights into the reaction mechanism, J. Phys. Chem. C 114 (2010) 1800–1804, https://doi.org/10.1021/jp9091305.
[11] B.K. Pong, H.I. Elim, J.X. Chong, W. Ji, B.L. Trout, J.Y. Lee, New insights on the nanoparticle growth mechanism in the citrate reduction of gold(III) salt: formation of the Au nanowire intermediate and its nonlinear optical properties, J. Phys. Chem. C 111 (2007) 6281–6287, https://doi.org/10.1021/jp068666o.
[12] V. Sanna, N. Pala, G. Dessì, P. Manconi, A. Mariani, S. Dedola, M. Rassu, C. Crosio, C. Iaccarino, M. Sechi, Single-step green synthesis and characterization of gold-conjugated polyphenol nanoparticles with antioxidant and biological activities, Int. J. Nanomed. 9 (2014) 4935–4951, https://doi.org/10.2147/IJN.S70648.
[13] S. Zhu, L. Zhu, J. Yu, Y. Wang, B. Peng, Anti-osteoclastogenic effect of epigallocatechin gallate-functionalized gold nanoparticles in vitro and in vivo, Int. J. Nanomed. 14 (2019) 5017–5032, https://doi.org/10.2147/IJN.S204628.
[14] N. Gan, C. Wakayama, S. Inubushi, T. Kunihisa, S. Mizumoto, M. Baba, H. Tanino, T. Ooya, Size dependency of selective cellular uptake of epigallocatechin gallate-modified gold nanoparticles for effective radiosensitization, ACS Appl. Bio Mater. 5 (2022) 355–365, https://doi.org/10.1021/acsabm.1c01149.
[15] C.C. Chen, D.S. Hsieh, K.J. Huang, Y.L. Chan, P. Da Hong, M.K. Yeh, C.J. Wu, Improving anticancer efficacy of (-)-epigallocatechin-3-gallate gold nanoparticles in murine B16F10 melanoma cells, Drug Des. Dev. Ther. 8 (2014) 459–473, https://doi.org/10.2147/DDDT.S58414.
[16] S.R. Chavva, S.K. Deshmukh, R. Kanchanapally, N. Tyagi, J.W. Coym, A.P. Singh, S. Singh, Epigallocatechin gallate-gold nanoparticles exhibit superior antitumor activity compared to conventional gold nanoparticles: potential synergistic interactions, Nanomaterials 9 (2019), https://doi.org/10.3390/nano9030396.
[17] D.S. Hsieh, H. Wang, S.W. Tan, Y.H. Huang, C.Y. Tsai, M.K. Yeh, C.J. Wu, The treatment of bladder cancer in a mouse model by epigallocatechin-3-gallate-gold nanoparticles, Biomaterials 32 (2011) 7633–7640, https://doi.org/10.1016/j.biomaterials.2011.06.073.
[18] O. Oladimeji, J. Akinyelu, A. Daniels, M. Singh, Modified gold nanoparticles for efficient delivery of betulinic acid to cancer cell mitochondria, Int. J. Mol. Sci. 22 (2021), https://doi.org/10.3390/ijms22105072.
[19] M.Y. Chang, A.L. Shiau, Y.H. Chen, C.J. Chang, H.H.W. Chen, C.L. Wu, Increased apoptotic potential and dose-enhancing effect of gold nanoparticles in combination with single-dose clinical electron beams on tumor-bearing mice, Cancer Sci. 99 (2008) 1479–1484, https://doi.org/10.1111/j.1349-7006.2008.00827.x.
[20] R. Shukla, N. Chanda, A. Zambre, A. Upendran, K. Katti, R.R. Kulkarni, S.K. Nune, S.W. Casteel, C.J. Smith, J. Vimal, E. Boote, J.D. Robertson, P. Kan, H. Engelbrecht, L.D. Watkinson, T.L. Carmack, J.R. Lever, C.S. Cutler, C. Caldwell, R. Kannan, K.V. Katti, Laminin receptor specific therapeutic gold nanoparticles (198AuNP-EGCg) show efficacy in treating prostate cancer, Proc. Natl. Acad. Sci. U.S.A. 109 (2012) 12426–12431, https://doi.org/10.1073/pnas.1121174109.
[21] W.H. De Jong, W.I. Hagens, P. Krystek, M.C. Burger, A.J.A.M. Sips, R.E. Geertsma, Particle size-dependent organ distribution of gold nanoparticles after intravenous administration, Biomaterials 29 (2008) 1912–1919, https://doi.org/10.1016/j.biomaterials.2007.12.037.
[22] G. Sonavane, K. Tomoda, K. Makino, Biodistribution of colloidal gold nanoparticles after intravenous administration: effect of particle size, Colloids Surf. B Biointerfaces 66 (2008) 274–280, https://doi.org/10.1016/j.colsurfb.2008.07.004.
[23] R. Terg, C.D. Miguez, L. Castro, H. Araldi, S. Dominguez, M. Rubio, Pharmacokinetics of Dextran-70 in patients with cirrhosis and ascites undergoing therapeutic paracentesis, J. Hepatol. 25 (1996) 329–333, https://doi.org/10.1016/S0168-8278(96)80119-X.
[24] S.L. Easo, P. V Mohanan, Hepatotoxicity evaluation of dextran stabilized iron oxide nanoparticles in Wistar rats, Int. J. Pharm. 509 (2016) 28–34, https://doi.org/10.1016/j.ijpharm.2016.05.026.
[25] X. Zhang, M.R. Servos, J. Liu, Ultrahigh nanoparticle stability against salt, pH, and solvent with retained surface accessibility via depletion stabilization, J. Am. Chem. Soc. 134 (2012) 9910–9913, https://doi.org/10.1021/ja303787e.
[26] Y. Zhao, F. Li, M.T. Carvajal, M.T. Harris, Interactions between bovine serum albumin and alginate: an evaluation of alginate as protein carrier, J. Colloid Interface Sci. 332 (2009) 345–353, https://doi.org/10.1016/j.jcis.2008.12.048.
[27] L. Ding, C. Yao, X. Yin, C. Li, Y. Huang, M. Wu, B. Wang, X. Guo, Y. Wang, M. Wu, Size, shape, and protein corona determine cellular uptake and removal mechanisms of gold nanoparticles, Small 14 (2018) 1–13, https://doi.org/10.1002/smll.201801451.
[28] G. Maiorano, S. Sabella, B. Sorce, V. Brunetti, M. Ada Malvindi, R. Cingolani, P. Paolo Pompa, Effects of cell culture media on the dynamic formation of Protein−Nanoparticle complexes and influence on the cellular response, ACS Nano 4 (2010) 7481–7491, https://doi.org/10.1021/nn101557e.
[29] X. Zheng, H. Baker, W.S. Hancock, F. Fawaz, M. McCaman, E. Pungor, Proteomic analysis for the assessment of different lots of fetal bovine serum as a raw material for cell culture. Part IV. Application of proteomics to the manufacture of biological drugs, Biotechnol. Prog. 22 (2006) 1294–1300, https://doi.org/10.1021/bp060121o.
[30] U. Sakulkhu, M. Mahmoudi, L. Maurizi, G. Coullerez, M. Hofmann-Amtenbrink, M. Vries, M. Motazacker, F. Rezaee, H. Hofmann, Significance of surface charge and shell material of superparamagnetic iron oxide nanoparticle (SPION) based core/shell nanoparticles on the composition of the protein corona, Biomater. Sci. 3 (2015) 265–278, https://doi.org/10.1039/c4bm00264d.
[31] R. Guo, R. Li, X. Li, L. Zhang, X. Jiang, B. Liu, Dual-functional alginic acid hybrid nanospheres for cell imaging and drug delivery, Small 5 (2009) 709–717, https://doi.org/10.1002/smll.200801375.
[32] S. Garabagiu, A spectroscopic study on the interaction between gold nanoparticles and hemoglobin, Mater. Res. Bull. 46 (2011) 2474–2477, https://doi.org/10.1016/j.materresbull.2011.08.032.
[33] I.F. Tannock, D. Rotin, Acid pH in tumors and its potential for therapeutic exploitation, Cancer Res. 49 (1989) 4373–4384.
[34] S. Amara, V. Tiriveedhi, Inflammatory role of high salt level in tumor microenvironment (Review), Int. J. Oncol. 50 (2017) 1477–1481, https://doi.org/10.3892/ijo.2017.3936.
[35] E. Sahin, A.O. Grillo, M.D. Perkins, C.J. Roberts, Comparative effects of pH and ionic strength on protein–protein interactions, unfolding, and aggregation for IgG1 antibodies, J. Pharmaceut. Sci. 99 (2010) 4830–4848, https://doi.org/10.1002/jps.22198.
[36] Y.T. Ho, N. 'Ain Azman, F.W.Y. Loh, G.K.T. Ong, G. Engudar, S.A. Kriz, J.C.Y. Kah, Protein corona formed from different blood plasma proteins affects the colloidal stability of nanoparticles differently, Bioconjugate Chem. 29 (2018) 3923–3934, https://doi.org/10.1021/acs.bioconjchem.8b00743.